Arabian Journal of Chemistry (2021) **14**, 103323

King Saud University

Arabian Journal of Chemistry

www.ksu.edu.sa
www.sciencedirect.com

ORIGINAL ARTICLE

Green synthesis of Ag nanoparticles in oil-in-water nano-emulsion and evaluation of their antibacterial and cytotoxic properties as well as molecular docking

Razieh Razavi [a], Mahnaz Amiri [b,c,*], Hassan Abbas Alshamsi [d], Tuba Eslaminejad [e], Masoud Salavati-Niasari [f,*]

[a] *Department of Chemistry, Faculty of Science, University of Jiroft, Jiroft, Iran*
[b] *Neuroscience Research Center, Institute of Neuropharmacology, Kerman University of Medical Science, Kerman, Iran*
[c] *Cell Therapy and Regenerative Medicine Comprehensive Center, Kerman University of Medical Science, Kerman, Iran*
[d] *Department of Chemistry, College of Education, University of Al-Qadisiyah, Diwaniya 1753, Iraq*
[e] *Pharmaceutics Research Center, Institute of Neuropharmacology, Kerman University of Medical Science, Kerman, Iran*
[f] *Institute of Nano Science and Nano Technology, University of Kashan, P.O. Box 87317-51167, Kashan, Islamic Republic of Iran*

Received 27 May 2021; accepted 8 July 2021
Available online 21 July 2021

KEYWORDS

Silver nanoparticle;
Green synthesis;
Antibacterial activity;
Cytotoxicity;
Herbal extract;
Molecular docking

Abstract Increasing use of silver nanoparticles (AgNPs) in various fields as mentioned recently like cosmetology, clinical nanotechnologies and medicine causes the growth of a nontoxic and green synthesis methodology. The present study provided a facile stable one-step synthesis of AgNPs in the presence of *Artemisia herba-alba*, *Mentha*, *Rosmarinus* and *Ranunculus* aqueous oil extract as reductant and stabilizer via oil-in-water nano-emulsion. Due to experimental results, in the presence of *Artemisia herba-alba* extract, AgNPs indicated smaller size, uniform shape and well dispersed NPs. Synthesized nanostructures characterized by using various techniques like XRD, UV–Vis, FT-IR, TEM, SEM, nano sizer and zeta potential measurements. The effect of some reaction parameters (the molar ratio of $AgNO_3$, extract volume, pH and temperature) on the AgNPs investigated as well. Additionally, strong antibacterial effects of AgNPs found against four gram-negative and three gram-positive bacteria due to cell death according to increasing membrane permeability and bacterial wall integrity disruption. WST-1 exposed cytotoxicity potent index on the

* Corresponding authors at: Neuroscience Research Center, Institute of Neuropharmacology, Kerman University of Medical Science, Kerman, Iran (M. Amiri); Tel.: +98 31 55912383; Fax: +98 31 55913201 (M. Salavati-Niasari).
E-mail addresses: ma.amiri@kmu.ac.ir (M. Amiri), salavati@kashanu.ac.ir (M. Salavati-Niasari).
Peer review under responsibility of King Saud University.

Production and hosting by Elsevier

https://doi.org/10.1016/j.arabjc.2021.103323

cancerous cell lines as established by the low IC50 value of 1 ppm. Binding energy of Ag metal with bacteria calculated by molecular docking and indicated that all bacteria have good interaction with silver NPs and confirmed antibacterial manner of Ag. Therefore, Produced AgNPs can be introduced as an effective antibacterial agent as well as a potent index of cytotoxicity effect on cancerous cell lines that leads to effective usage in nono-drug design and formulations in near future.

1. Introduction

Currently, nanotechnology is concerned as an advanced scientific field which contains numerous size of synthesis nanoparticles, shapes and chemical structures with diverse potential applications (Beg et al., 2016). Numerous procedures for heavy noble metals such as Pd, Pt, Au and Ag nanoparticle preparation have been stated in the literatures (Jiang and Pinchuk, 2015). Silver nanoparticles (AgNPs), amongst all noble metal nanoparticles, indicate key role owing to not only their unique structural, but also for plasmonic as well as physical chemistry properties counting functionalization of surface and controlled drug release (Kumar et al., 2017; Ahmed et al., 2016). AgNPs exhibit high antimicrobial usefulness as a result of their thermal stability, large area of solution surface for reserving Ag^+ and Ag^+ release rate, which is reliant on the various factors like geometric shape, type and size of silver NPs, besides of approaches of synthesis (Solmon and Umoren, 2016). As cosmetic preservative compounds; phenoxyethanol and paraben stimulate the skin condition temporarily and increase the sensitivity of ultraviolet (UV) light (Ishiwatari et al., 2007). Silver and Ag complexes had been applied for growth controlling of bacteria in various works (Silver et al., 2006). Chemical reduction (Bastús et al., 2014), microwave irradiation (Bahadur et al., 2011); photoreduction (Kshirsagar et al., 2011), thermal decomposition (Daengsakul et al., 2009) reported as different methods for the synthesis of nanoparticles and nanoparticles design that these processes are largely energy intensive and expensive for environment and human health. Accordingly, environmentally friendly had be established (Naghdi et al., 2015). Green synthesis suggests physical and chemical development in processes like as environment friendly, cost effective, certainly scaled up without high pressure for large scale synthesis, temperature, energy as well as toxic substances. Enzymes, plant extracts and microorganisms are used for metal ions bioreduction by getting chemical complexes (Rani and Rajasekharredy, 2011) extremely. The plant-mediated synthesis, amongst the several green synthesis techniques, seems to be a favorable process that leads to nanoparticles synthesis by consuming less times and facilitates for stable synthesis (Amiri et al., 2017). This bio-inspired nanoparticles synthesis gained much attention and methodologies for controlling the nanoparticles size (Amiria et al., 2018). Plant's biomolecules were displayed an important role in formation of nanoparticles with different sizes and morphologies that have making eco-friendly procedures development in nanoparticle synthesis (Amiri et al., 2017). Wide range of enormous biomolecules played capping and reducing action in the nanoparticles synthesis (Raja et al., 2017). Numerous plants which contain natural biosurfactant molecules with enough foaming, wetting and oil dispersion have nonionic triterpenoid glycosides (hydrophobic part) and the ionic part (hydrophilic) of biosurfactant includes sugars (Sura et al., 2018). All parts of plants (flowers, bark, leaves, fruits and seeds) had been applied for synthesizing of nanoparticles (Majeed et al., 2016). Recent reports indicated plant synthesis of silver nanoparticles using floral extracts of *Calotropisprocera* (Babu and Prabu, 2011); *Hibiscus rosa-sinensis* (Surya et al., 2016) and *Delonixelata* (Valli and Suganya, 2015) *Artemisia herba-alba*. Desert wormwood is an aromatic dwarf shrub and medicinal which is going from the *Asteraceae* family, *Anthemideae* tribe (Tilaoui et al., 2011) and *genus Artemisia* that grows widely in Mediterranean region where spreading to north-western Himalayas, middle east and India (Vernin et al., 1995). The essential oil of *A. herba-alba* known as armoise oil is traditional medicine archaeologically. There are various pharmacological and biological effects in armoise oil (Hudaib and Aburjai, 2006). *Ranunculus* plants stay alive in several environments, from cold alpine mountains to low-lying wetlands. This genus offers different physiology and morphology and having an acceptable adaptability. 78 species and 9 varieties of Flora *of China* are dispersed in China extremely (Emadzade et al., 2011). In the Lamiaceae family *Mentha* is a famous genus which include 25–30 types that are broadly grownup in temperate zones, principally in Europe, Asia Minor, North Africa, near East (Syria, Ethiopia) and Northern parts of Iran but currently, it exists all over regions of the world (Singh et al., 2015). Rosemary (*Rosmarinus officinalis)* is a perennial herb and woody that related to the Mediterranean region.

At this point, we report an unprecedented green synthetic oil-in-water nano-emulsion method comprising production of silver nanoparticles (AgNPs) using the *Artemisia herba-alba, Mentha, Rosmarinus* and *Ranunculus* aqueous extract. The structure, morphology of the synthesized AgNPs and particle size were studied using various spectroscopic techniques. Furthermore, cosmetic preparations and pharmaceutical usage of Ag nanoparticles were caused to investigate the antimicrobial activity of Ag nanoparticles against a wide range of microorganisms and to identify safety usage of Ag nanoparticles for skin (cytotoxicity investigations). This study is novel to recognize the nanobiotechnological potential of these extracts for AgNPs synthesis that has not been reported earlier. Molecular docking supported the investigation as well.

2. Materials and methods

2.1. Materials

Whole chemical materials which had analytical purity applied for this research without extra purification process. Silver nitrate ($AgNO_3$, 99%) was purchased from Merck Company (Pvt. Ltd.), Germany. Reagents and standard laboratory chemicals were prepared from the Sigma-Aldrich Company, USA that includes penicillin–streptomycin (100 μg/ml), Dulbecco's modified eagle's medium, fetal bovine serum (FBS), phosphate-buffered saline (PBS), trypsin- EDTA solution, dimethyl sulfoxide, trypan blue dye solution, iodonitrotetrazolium (INT), Ciprofloxacin. 2-(2-methoxy-4-nitrophenyl)-3-(4-nitrophenyl)-5-(2, 4-disulfophenyl)-2H-tetrazolium (WST-1 reagent) was prepared from Roche Holding AG. All eukaryote cells were prepared from Pasteur institute of Iran.

2.2. Essential oil extraction

Dark place and inert atmosphere used for drying herbal samples at room temperature for 15 days. Aerial parts and hydromethanol distilled in a Clevenger-type apparatus for 3 h in order to extract the essential oil. All experiments were extracted two times. Anhydrous sodium sulfate (Na_2SO_4) was used to dry essential oils and sealed vials used to store and to protect from light during analysis processes at 4 °C.

2.3. Green synthesis processes of silver nanoparticles

The syntheses were carried out in oil-in-water (O/W) nano-emulsions by mixing the right amounts of the reagents to obtain the desired composition. Typically, about 5 ml of various extracted oil solutions gradually added to 30 ml of 1.75 mM $AgNO_3$ solution in separated beakers, while stirring at 5000 rpm speed via a homogenizer at 40 °C. The color of reaction solutions were changed to light brown rapidly and turn into turbid. Then standing for overnight, the color of solution states dark brown. After the synthesis was finished, the nanoparticles were separated by centrifugation and subjected to several washings with acetone, ethanol and water and dried at 40 °C in a vacuum oven finally. The small droplet size of nano-emulsions confers stability against sedimentation (or creaming) because the Brownian motion and consequently the diffusion rate are higher than the sedimentation (or creaming) rate induced by the gravity force. Ostwald ripening or molecular diffusion, which a rises from emulsion polydispersity and the difference in solubility between small and large droplets, is the main mechanism for nano-emulsion destabilization (Tadros et al., 2004).

In order to optimize the AgNPs synthesis parameters, effect of some parameters like, different $AgNO_3$ concentrations (0.75, 1, 1.25, 1.5, 1.75 mM), extract volume (1, 2, 3, 4, 5 ml), temperature (27, 40, 60, 80 °C), and pH (8, 10 and 12) in the presence of different extracts was observed as well.

2.4. Microbial culture and antimicrobial effect of AgNPs

In order to investigate antimicrobial effect of nanostructures microbial cultures of *Bacillus subtilis* (ATCC 6051), *Micrococcus luteus (ATCC 4698), Staphylococcus aureus (ATCC 29213), Escherichia coli (ATCC 25922), Klebsiella pneumoniae* (ATCC 13883), *Proteus mirabilis (ATCC 21100)* and *Pseudomonas aeruginosa* (ATCC 27853) were chosen carefully. In order to obtain the aimed fresh cultures, the Mueller-Hinton agar was used to prepare them and overnighted at 37 °C in medium. A modified micro-dilution assay protocol was applied to determine the antibacterial effect (Elshikh et al., 2016). At first all microbial inoculums were prepared (0.5 McFarland) then preparation of the serial dilution (0.3–1000 μg/ml) of the silver nanoparticles were done in a 96-well round-bottom microplate. After that, microbial strains cultured and incubated at 37 °C for 24 h to desire well. After passing one day, 40 μl INT solution (0.6 mg/ml) was added to every well and incubated 20 min at 37 °C and the absorbance of each solution was read at 490 nm. Ciprofloxacin as positive control at 0.5–8 μg/ml concentration was used and blank was containing of all reagents except the bacteria, culture medium was used as the negative control. Below equation was applied to calculate the mortality rate (%) (Eslaminejad et al., 2016): Mortality rate (%) = ((A − C)/(B − C)) × 100; Where A = Test sample; B = positive control; C = negative control.

2.5. Computational method

Protein Data Bank (PDB) (www.rcsb.org) used for preparing crystal structures of bacteria. Amber force field selected for minimizing the docking process. Molecular docking experiment was employed by AutoDock4. The grid box parameters values were used to as center 33.4238, center 9.4981, center 28.8764 in x, y, and z direction respectively. Then binding energy of docking calculated by low RMSD evaluation by The Lamarckian genetic algorithm and graphical presentation has been done by using Discovery Studio (2.1.0) (Accelrys Software Inc., 2007).

2.6. Cell culture and in vitro cytotoxicity

In vitro cytotoxicity investigated as our previous papers (Amiri et al., 2018). Briefly Human breast cancer (MCF-7) cells and 3T3 fibroblasts as a normal cell line was used and was incubated in 5% CO_2 at 37 °C and until flaunted the 75% of the culture plate. DMEM was used to grow cell lines that accompanied with 10% fetal bovine serum, penicillin–streptomycin (100 U/ml) and the medium replaced every other day. 24 h applied for incubating the 10,000 cells/well of each cell line on the 96 well plates. After one day the medium aspirated. 100 μl of various concentrations (4, 8, 16, 32, 64, 125, 250, 500 and 1000 μg/ml) poured to wells and the plates were kept overnight at 37 °C under 5% CO_2. After one day, 10 μl of solution of WST-1 was added to each well and was incubated for 4 h. The absorbance of solution read at 420 nm by ELISA reader (BioTeks Elx 800). Viability of cell was stated as 100% for untreated control cells. The survival rate (%) was calculated by below equation (Eslaminejad et al., 2016) and All samples were performed in triplicates: Survival rate (%) = (OD in treatment group/OD in control group) × 100. The inhibitory concentration required for 50% cytotoxicity (IC_{50}) value was determined. The optical density (MTT assay) was determined at 420 nm using a microplate reader (BioTeks Elx 800).

2.7. Characterization of Ag nanostructures

The range of 300–600 nm wavelength was used to measure UV–Vis spectra with a wavelength step size of 2 nm at room temperature by Optizen 3220 UV (Corea). A series of technologies for characterization of synthesized samples were applied. Fourier transform infrared (FT-IR) spectra were verified by Bruker, FT-IR alpha model. X-ray diffraction (XRD) were detailed by X-ray diffractometer using Ni-filtered Cu Kα radiation (Philips-X'pertpro). SEM (Scanning electron microscopy (LEO instrument model 1455VP)) and TEM (transmission electron microscope (Philips EM208, accelerating voltage of 200 kV)) were applied to recognize the morphologies of the made-up NPs. Vasco and Wallis model of Nanosizer cordouan (France) was applied to determination of particle size and zeta potential. pH measurements were done by an 827 lab pHmeter made by Metrohm Company.

2.8. Statistical analysis

Student's *t*-test and analysis of variances were applied to evaluated significance among groups. All data are represented as

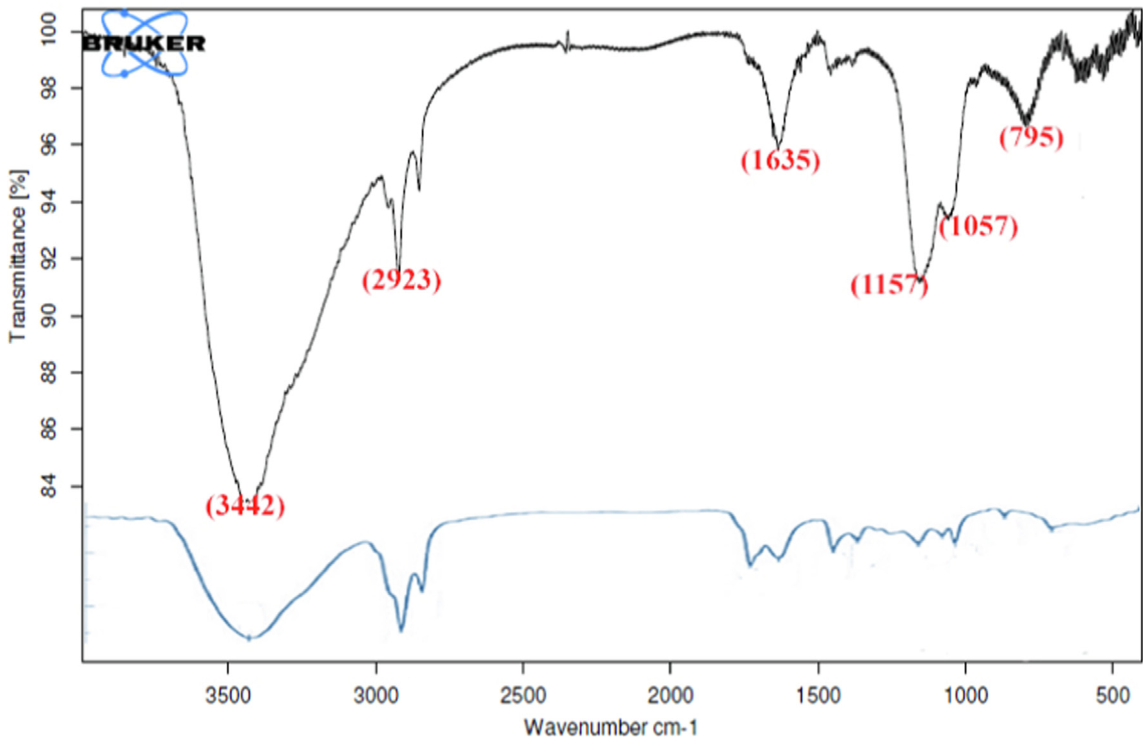

Fig. 1 FT-IR spectrum of green synthesized Ag nanostructures.

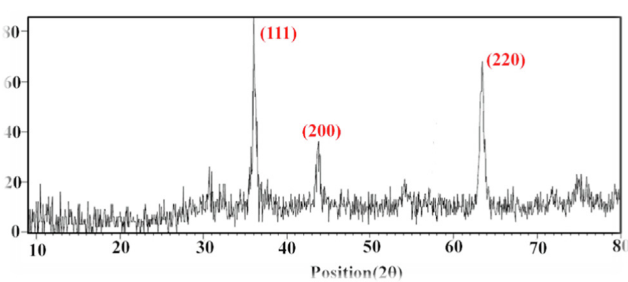

Fig. 2 X-ray diffraction pattern of green synthesized Ag nanostructures.

mean ± SD. The probability level of $p < 0.05$ was considered as statistical significance.

3. Results and discussion

In the present work, four aqueous extracts were applied for synthesizing of silver nanoparticles (AgNPs). Responsibility of reduction of Ag^+ ions to Ag^0 resulted from the biomolecules presented in the extracts in a single step.

$$AgNO_3 \rightarrow Ag^+ + NO_3^-$$

$$Ag^+ + \text{Extract} \rightarrow Ag^0$$

The bio-reduction of silver ions into AgNPs by using herbal extracts were demonstrated in Section 3.3. It is obvious from the obtained data that use of 5 ml of extracted oil and 1.75 mM of $AgNO_3$ is the optimal condition but about temperature 40 °C was selected because higher temperature did not produce more NPs and only use more energy source.

Due to synthesis of uniform, well dispersed and smaller size of AgNPs in the presence of *Artemisia herba-alba* extract, more characterization done on silver nanoparticles that prepared by using this extract.

3.1. Ag nanostructures characterization

Generally, FT-IR spectrum provides structural and functional groups information and molecular bonds nature in the substances. FT-IR spectroscopy applied to classify the functional groups that have controllable role for the bioreduction and capping of noble ion (Ag^+ to Ag^0) in this work, Fig. 1 exhibits the FT-IR spectra of synthesized AgNPs in herbal extract. The spectrum demonstrates bands at 3442, 2923, 1635, 1157, 1057 and 795 cm^{-1}. Mostly, expand peak in 3307–3325 cm^{-1} shows the presence of the OH stretching of phenolic and flavonoids mixtures, although AgNPs synthesized using the extract shows the same band at higher frequency (Dubey et al., 2010). Further, AgNPs displays the weak band at the 2923 cm^{-1} attributed to the alkenes C-H stretching vibration (Varadavenkatesan et al., 2017). The peak with sharp absorption intensity that was detected at the 1635 cm^{-1} can be pointed to the amide-I bond because of carbonyl-amide linkages stretching that is representing which proteins were interrelating with green synthesized AgNPs and their secondary structure has not affected during or afterward the reaction with Ag^+ ions. Strong binding ability was produced with amino acid residues (carbonyl function group) and metal (capping agent) which avoid agglomeration and provide medium stability (Boopathi et al., 2012). Moreover, the existence of aliphatic amines in proteins were represented by two bands between 1157 and 1057 cm^{-1} vibration of C-N stretching. The band peak at the 795 cm^{-1}

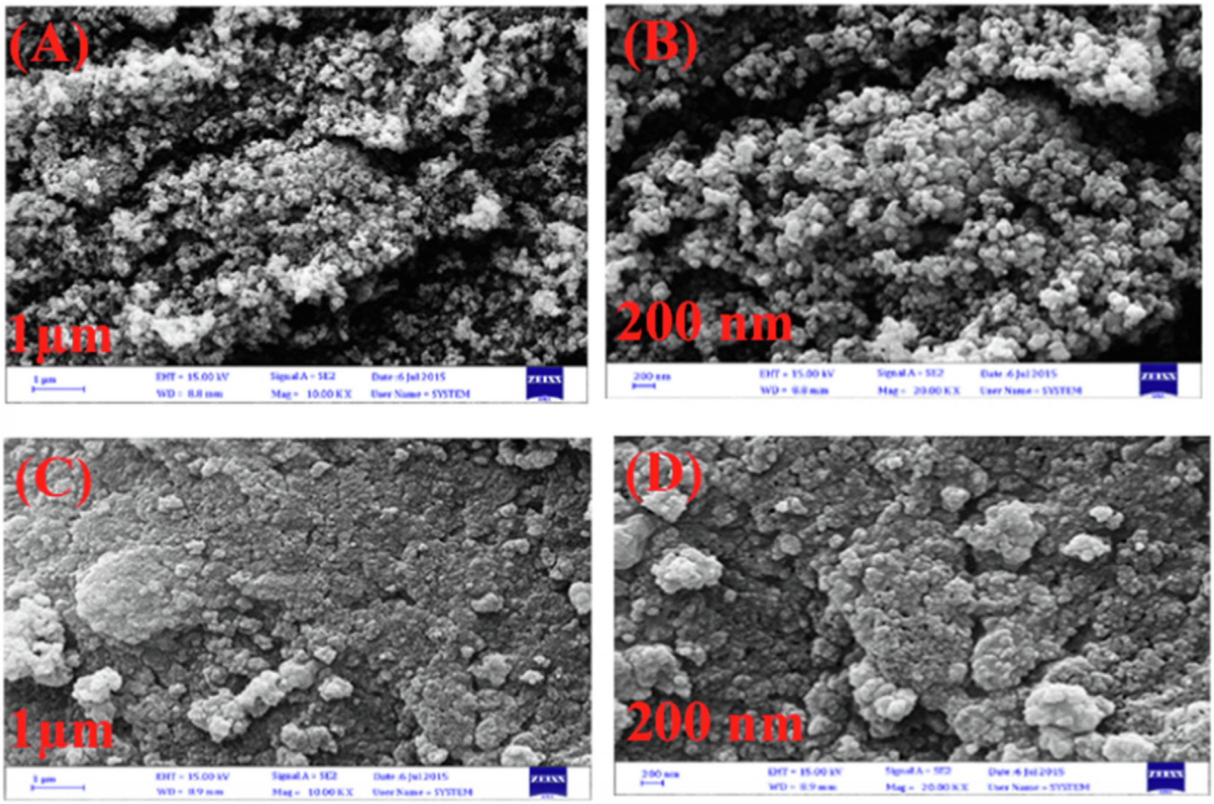

Fig. 3 Scanning electron microscopy (SEM) of AgNPs synthesized in the presence of *Artemisia herba-alba* extract at pH of 10 (A, B) and pH of 12 (C, D).

states heterocyclic compounds that related to present flavonoids (Kacurakova et al., 2000). Observed data verifies action of proteins as coating/stabilizing agent and antioxidants reducing agent like as flavonoids/phenolic compounds. XRD technique has applied to analyze the crystal structure nature of the synthesized AgNPs. Multiple strong peaks recognized at (1 1 1), (2 0 0) and (2 2 0) of the face centered cubic lattic that resulted crystal structure of Ag metal (Gogoi et al., 2015) (Fig. 2) which are consistent with Ag^0 standard (JCPDS Card no. 04–0783) (Coseri et al., 2015). The plane (1 1 1) was the major element of Ag planes. The average of crystallite size D can be obtained from the (1 1 1) peak in XRD patterns by driving in the Scherrer Equation (Amiri et al., 2016): $D = k\lambda/Bc$ $os\theta$; where B is the full-width at half maximum (FWHM) of a diffraction peak, k is the Scherrer constant (0.89), and θ is the Bragg's angle. The calculated crystal size by the XRD reflections is about 38 ± 2 nm. Nanosize range was indicated from the XRD lines according to sharper reflexes with improved intensity emerge, signifying the presence of a smaller nanocrystalline phase. Generally, Electrokinetic potential can be taken from zeta potential in colloidal dispersions scientifically. Measurements of Zeta potential were done and confirmed that the nanoparticles surface have a negative electric charge which let them to stay in colloidal suspension manner. Results established that the zeta potential of the AgNPs increases by increasing of extract content, therefore the higher content of extracted biomolecules (the herbal extract/$AgNO_3$ ratio of 5) present in the system, nanoparticles indicated the most negatively charged of −56 mV. The stability of the nanoparticles provided by negative charges which preventing aggregation and agglomeration.

The SEM images of synthesized NPs at two different pH are presented in Fig. 3(A-D). SEM image (Fig. 3A and B) evidently demonstrated that AgNPs were not agglomerated and are spherically shaped with a diameter ranging from 40 to 50 nm. By increasing the pH (the pH increased by gradually addition of 0.20 M NaOH solution) from 10 to 12 (Fig. 3C and D), AgNPs indicated spherical- to oval-shape with a larger average diameter and more agglomeration. It is possibly owing to the growth rate of AgNPs become faster than the nucleation rate with increasing the pH (Li et al., 2017). Extracted Biomolecules like proteins, enzymes, terpenoids and flavonoids cofactors play both capping and reducing role in the nanoparticles synthesis (Raja et al., 2017), Furthermore due to strong binding ability with amino acid residues (carbonyl group) with metal as capping agent, agglomeration behavior was prevented and stability of medium was provided (Boopathi et al., 2012).

Transmission electron microscopy images of AgNPs prepared at herbal extract, is shown in Fig. 4A and the size distribution from TEM images is presenrted. As shown, TEM images confirmed a spherical shaped and well-dispersion of nanostructures. The results were in good accommodation with the observation of SEM and XRD (scherrer equation) that approve the synthesis of AgNPs by a natural material (Arokiyaraj et al., 2014). For better understanding of the real size of nanoparticles, Nanosizer used for calculating particle size and stated by SBL (Statistical Bin Limits) analyze. For this propose, reduction of agglomeration fault to state actual particles size were done by omitting hydrodynamic radius. Fig. 4B reported the histogram of SBL nanosizer of NPs in which showed the mean diameter of size of particle is ~51.39 nm.

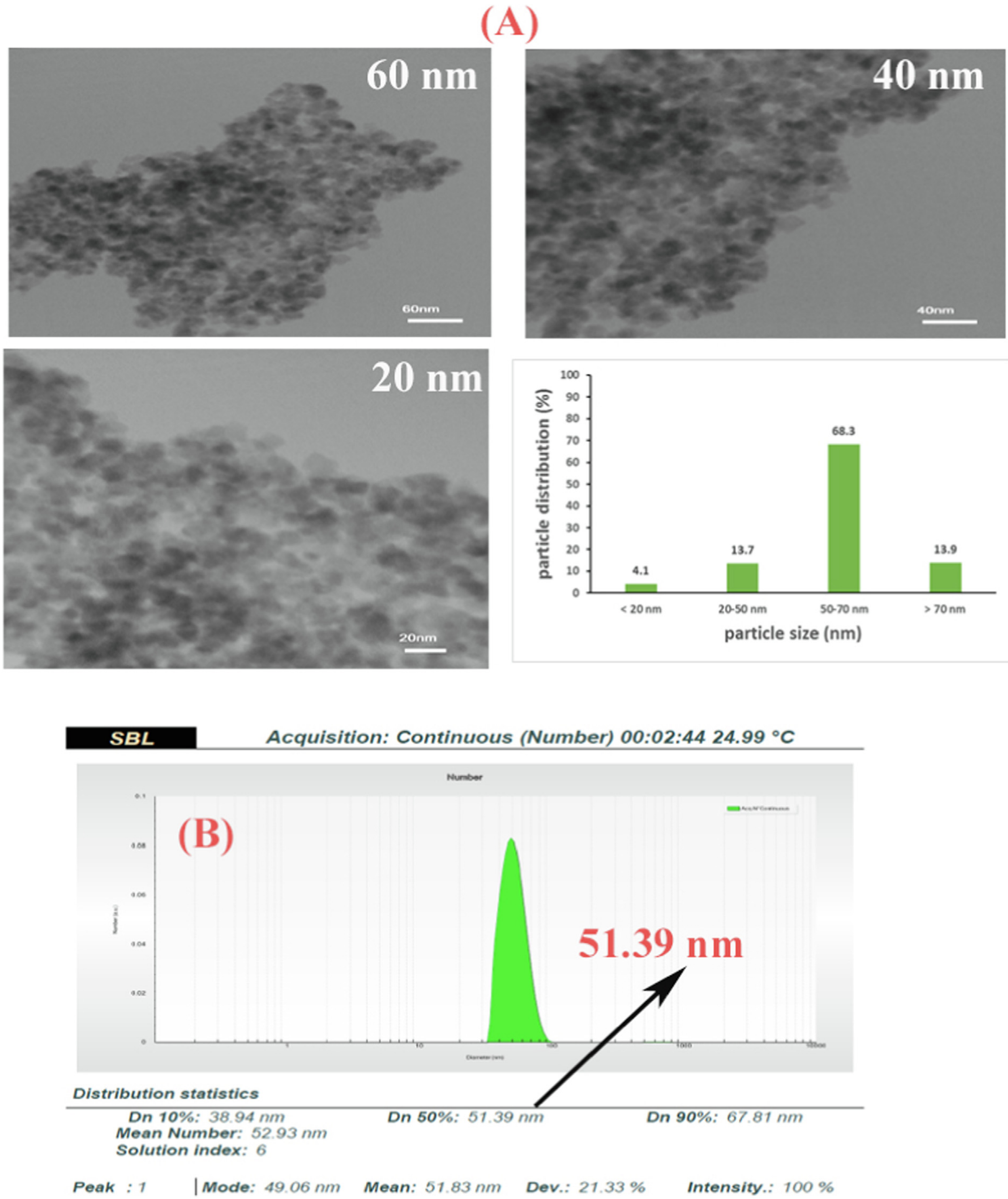

Fig. 4 TEM image of Ag nanostructures synthesized at pH 10 at different magnitude as well as size distribution of Ag NPs based TEM images (A), The SBL (Statistical Bin Limits) nanosizer histogram of NPs (B).

Reported results demonstrated narrow size distribution and homogenous dispersity of NPs.

3.2. Ag nanoparticles synthesis investigation

For Ag nanoparticles synthesis, the reaction mixture ($AgNO_3$ solution) entirely turned to brown after *Artemisia* extract addition at room temperature (Fig. 5A). The brown color of the reaction mixture corresponds to silver nanoparticles surface plasmonace that made in the reaction mixture. Mostly, UV–Vis spectroscopy can be employed for the detection of the appropriate size and distribution of AgNPs due to the surface plasmon resonance excitation (SPR) (Lee and Mooney, 2012). The UV–Vis spectra of the AgNPs prepared at different pH levels in the presence of Artemisia is revealed in Fig. 5B. The strongest symmetric absorbance band is positioned at approximately 420 and 415 nm (pH 8 and 10) and 395 nm (pH 12) in the UV–Vis spectra, demonstrative to the formation of well-

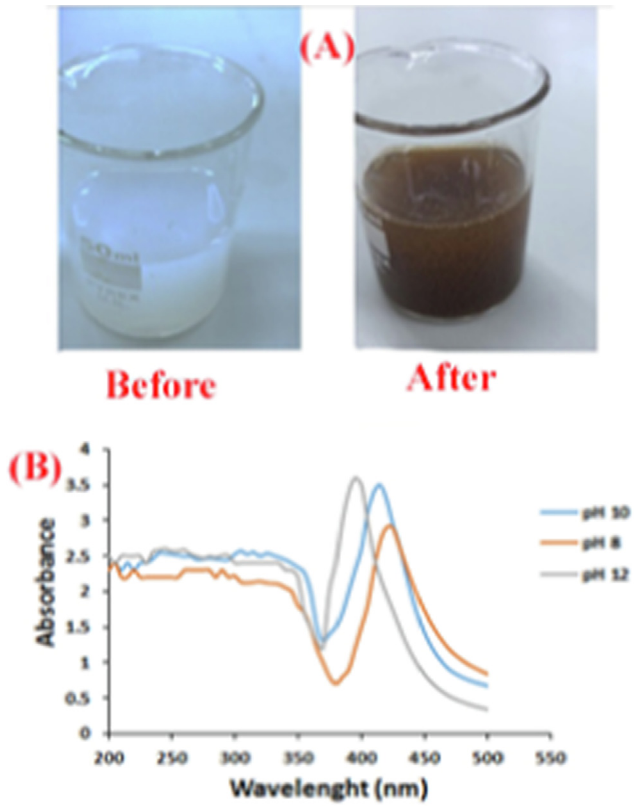

Fig. 5 Photographic image of reduction of Ag^{+} to Ag^{0} before and after addition of herbal extract (A), UV–Vis spectra of pH dependent synthesis of silver nanoparticles in the presence of *Artemisia herba-alba extract* (B).

dispersed Ag NPs. With increasing pH value, the absorption peak intensity steadily increased, once the pH value reached 12, the band obviously shifted toward lower wavelengths. The higher pH value would make the alkaline hydrolysis to produce smaller molecular masses of fragments with higher reducibility and affinity, which are essential for the well-dispersed and stable AgNPs synthesis. Additionally, the silver salt concentration and extract volume are another factors that can excellently modify the silver nanoparticles shape. Fig. 6A and 6B demonstrate the UV–Vis spectra of silver nanoparticles prepared by different concentrations of $AgNO_3$ and herbal extracts volume respectively. When the concentration of Ag salt increases to 1.75 mM, a very identical style in the nanoparticles synthesis was detected for all investigated media. The adsorption peak strength increases with the increasing the content of metallic precursors and similarly by increasing the herbal extracts amount, consequently a displacement to longer wavelengths is observed in the UV–Vis spectrum of the nanoparticles synthesized with a higher metallic precursor content (figure not shown). The results demonstrate that by increasing $AgNO_3$ concentration, the peak intensity increased for all samples as well. No significant effect of increasing the extract was observed in *Mentha* while silver nanostructures synthesized in the presence of other extracts designated more adsorption peak intensity. In addition, the effect of varying temperature (Fig. 6C) was more significant for AgNPs synthesized in the presence of *Rosmarinus* and *Mentha* that by increasing temperature reduction in adsorption peaks revealed that possibly is due to the AgNPs aggregation. However, at 80 °C *Ranunculus* presented relatively (1.4 folds) higher synthesis, while *Artemisia* exhibited the highest one. These results suggested better efficacy of *Rosmarinus* particularly, even at lower temperature in comparison with other extracts.

3.3. Ag nanoparticles antimicrobial evaluation

Antibiotic resistance is one of the main public health concerns of this century. This resistance is also associated with oxidative stress, which could contribute to the selection of resistant bacterial strains. Antimicrobial evaluation of the green synthesized silver nanoparticles was investigated on the four gram-negative, and three gram-positive including *E. coli*, *K. pneumonia*, *P. mirabilis*, *P. aeruginosa*, *M. luteus, B. subtilis,* and *S. aureus*. The bactericidal properties of AgNPs depends on their stability in the growth medium, the capping agents and the shape/size of AgNPs which plays an important role in improving their antimicrobial properties (Pal et al., 2007). Overall, acceptable antimicrobial activity of Ag NPs is due to smaller size and higher surface to volume ratio of NPs which permits the presence of active Ag atoms on their surface, leading to enhanced antimicrobial activity (Ocsoy et al., 2017). Obtained results presented that the antimicrobial activity varied between the microbial strains. Both of the gram positive and negative bacteria were sensitive to the test samples. The MIC_{50} values for this synthesized nanoparticle were 8, 4, 4, 2, 2, 1 and 4 ppm, for the investigated bacteria; *E. coli*, *K. pneumonia*, *P. mirabilis*, *P. aeruginosa*, *M. luteus, B. subtilis,* and *S. aureus*. respectively as seen in the following Fig. 7A and B. Although there is a distinct variance between the activities of the AgNPs in the case of the 7 bacteria strains, the antimicrobial activity in the case of *B. subtilis* is noticeably higher compared to the other ones. The effect of silver particles against bacteria is due to their interaction with thiol group compounds, which are found in the bacterial cells respiratory enzymes. It was reported earlier that, Silver binds to the bacterial cell wall and cell membrane that hinders the respiration process, due to the much larger surface area, AgNPs demonstrate increased antimicrobial activity, AgNPs get attached to the bacterium cell membrane and also penetrate the bacteria inside. The bacterial membrane covers sulfur-containing proteins and the silver nanoparticles act together with these proteins in the cell as well as with the phosphorus containing compounds like DNA. AgNPs preferably attack the respiratory chain (Rai et al., 2009; Singh et al., 2015).

3.4. Ag nanoparticles cytotoxicity studies

WST-1 assay was performed for calculating of AgNPs cytotoxicity against the MCF-7 cells and 3T3 cell lines (Fig. 8B). In cultured cells, viability was meaningfully reduced in the presence of AgNPs at several concentrations that suggested a dose-dependent manner. The silver NPs revealed a potent index of cytotoxicity effect on cancerous and normal cell line as verified by the low IC_{50} value of 1 ppm (Fig. 8B). The inhibitory effects of AgNPs on the breast cancer cells may be due to the characteristics of this disease, so that the cells of this cancer illustrate a higher rate of metabolism, quick cell division, and consequently exhibit improved internalization of AgNPs, causing in a higher cell death rate. Also, other studies

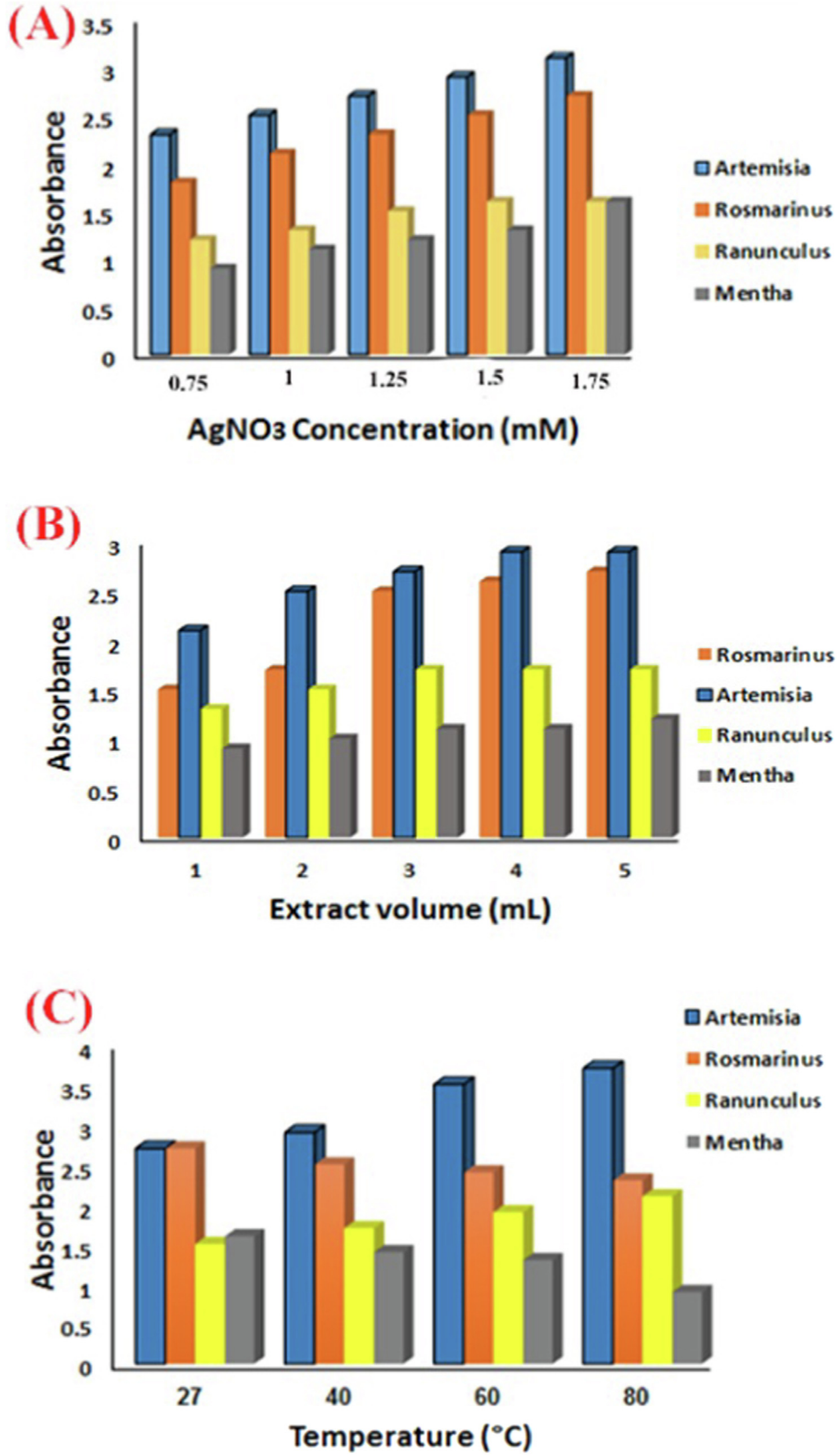

Fig. 6 Various $AgNO_3$ concentration effect (A) extract volume (B) and temperature (C) on production of AgNPs using various aqueous extracts respectively.

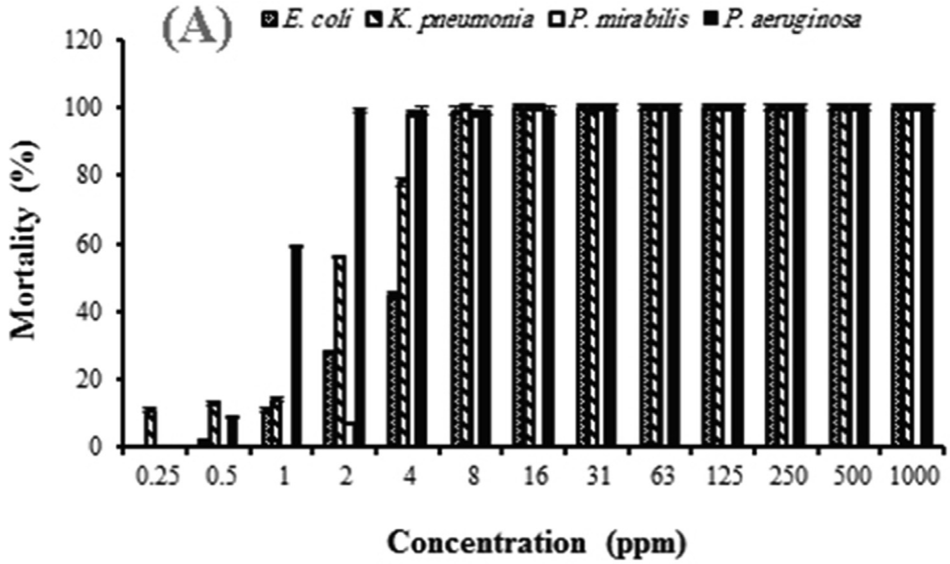

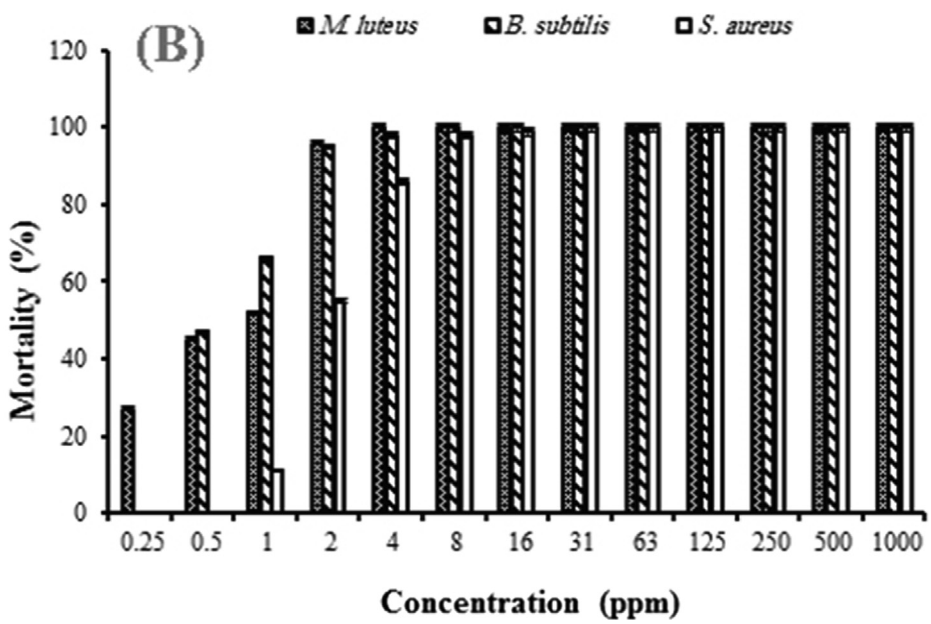

Fig. 7 Mortality (%) of the green synthesized silver nanoparticles on the gram-negative bacteria (A) and on the gram-positive bacteria (B).

established AgNPs at the concentrations above 2 μg Ag/mL displayed to be harmful/cytotoxic for the MCF-7 cells (Roszak et al., 2017). The decreased cell viability against AgNPs is because of not only generation of reactive oxygen species, but also decreased cellular ATP content as well as reduced dehydrogenase activity that does damage to mitochondrial respiratory chain and cellular components resulting in cell death (Justin Packia Jacob et al., 2012). Hence, cytotoxicity of phytogenic AgNPs is dependent on cell type that demonstrates a specific intracellular mechanism for proliferation inhibition rather than an unspecific disturbance of cell membrane functionality. However, cytotoxicity of NPs is exclusively based on their shape, size, surface chemistry, interaction time and agglomeration state (Rajkuberan et al., 2015).

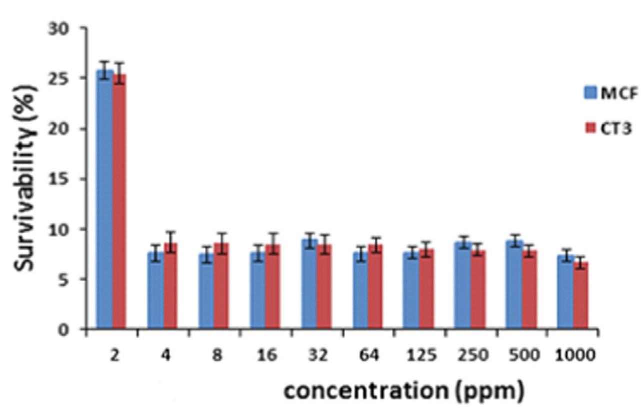

Fig. 8 The cytotoxicity investigation of AgNPs on MCF and 3T3 cell lines.

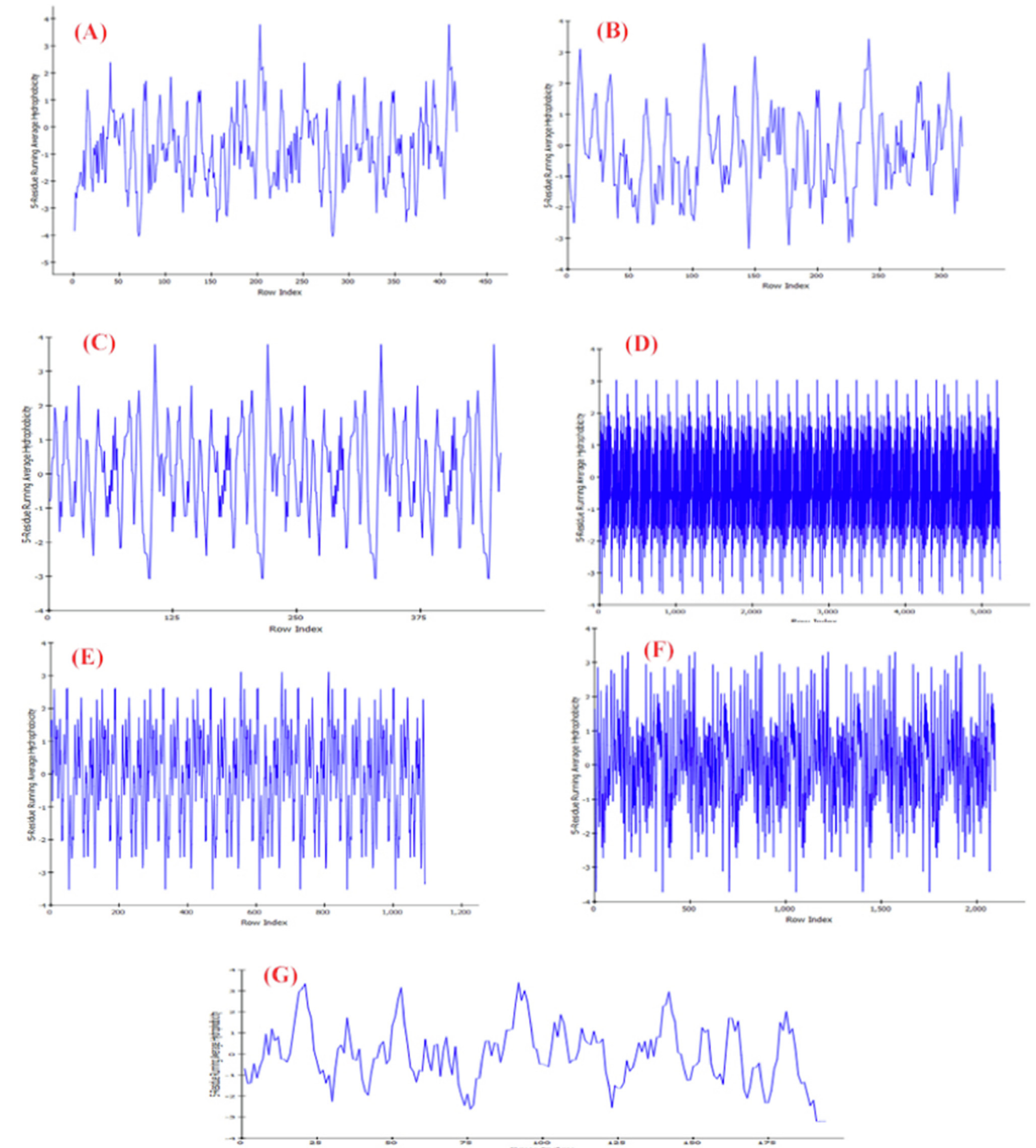

Fig. 9 Hydrophobicity plot of (A) Staphylococcus aureus, (B) Escherichia coli, (C) Pseudomonas aeruginosa, (D) Bacillus subtilis, (E) Klebsiella pneumoniae, (F) Micrococcus luteus, (G) Proteus mirabilis.

3.5. Ag nanoparticles docking finding

Protein Data Bank (PDB) (www.rcsb.org) used for preparing crystal structures of bacteria. Amber force field selected for minimizing the docking process. Molecular docking experiment was employed by AutoDock4 (Rizwan, 2012). The grid box parameters values was used to as center 33.4238, center 9.4981, center 28.8764 in x, y, and z direction respectively. Then binding energy of docking calculated by low RMSD evaluation by the Lamarckian genetic algorithm and graphical presentation has been done by using Discovery Studio (2.1.0) (Kyte and Doolittle, 1982).

Hydrophobicity of proteins, amino acids and microbiological structure such as bacteria cause the ability of water proof-

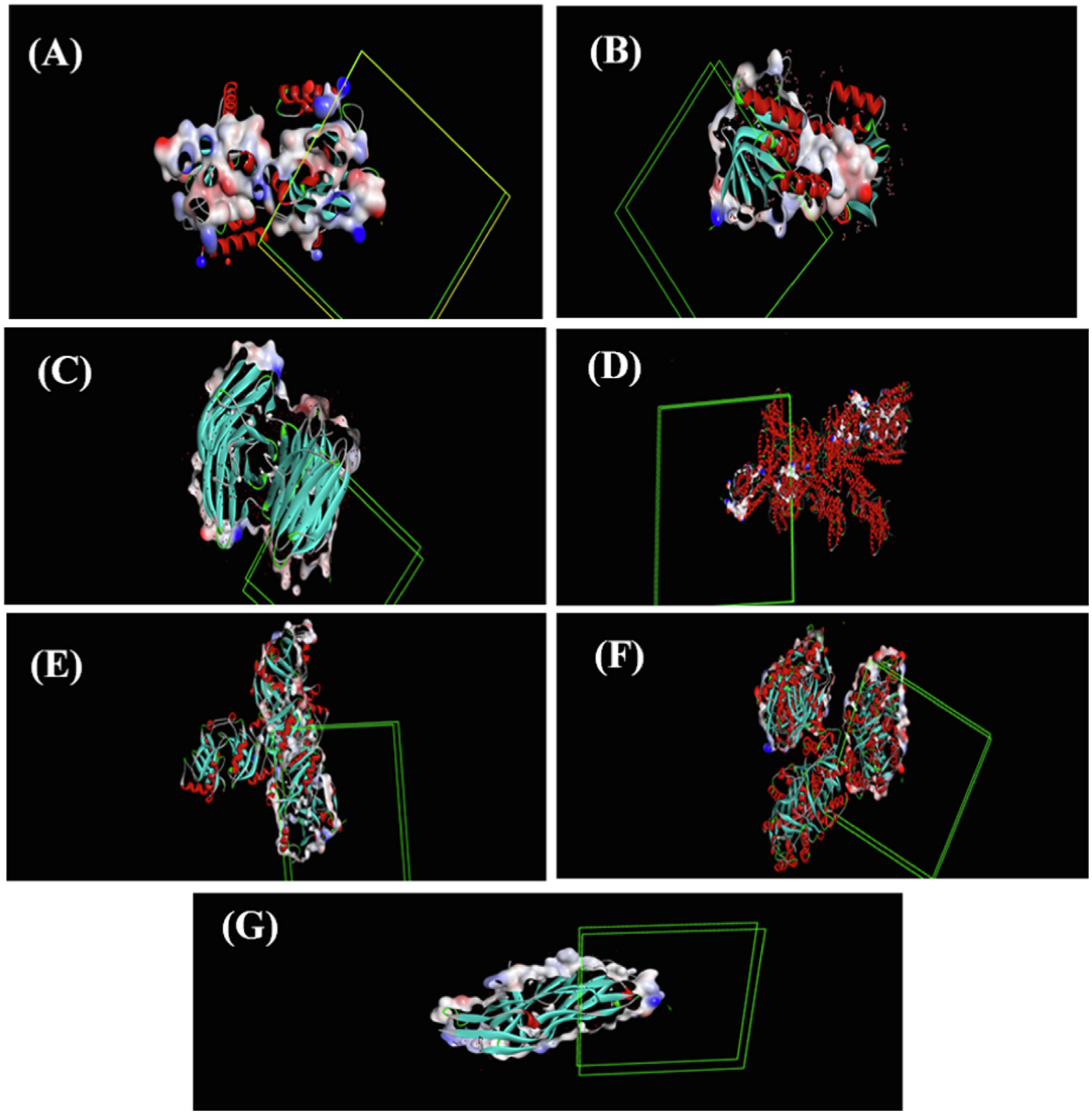

Fig. 10 Electron density surface and pose of binding with Ag nanostructures of (A) Staphylococcus aureus, (B) Escherichia coli, (C) Pseudomonas aeruginosa, (D) Bacillus subtilis, (E) Klebsiella pneumoniae, (F) Micrococcus luteus, (G) Proteus mirabilis.

Table 1 Docking energy values ΔG in kcal/mol of Ag interaction with bacteria.

Compound	Docking Energy kcal/mol
Proteus mirabilis	−6.73
Micrococcus luteus	−6.23
Klebsiella pneumoniae	−7.45
Bacillus subtilis	−3.25
Staphylococcus aureus	−6.78
Escherichia coli	−7.89
Pseudomonas aeruginosa	−5.20

ing in biochemistry. This effect indicate the hydrogen bonding in structure (Morris et al., 2009). A hydrophilicity plots Fig. 9(A-G) are a quantitative analysis of the degree of hydrophobicity or hydrophilicity of amino acids of bacteria's that applied in this study. The figures indicated all bacteria have interaction by polar solvents with special amino acids. All plots showed that parts of alpha helix with positive hydrophobicity are contained amino acids. Therefore amino acids with high hydrophilicity indicate which these residues are in contact with solvent and they are therefore likely to reside on the outer surface of the protein (Accelrys Software Inc., 2007). Electron density surface is a real place which chemical compounds have ability to accept the other structures. In Fig. 10(A-G) surface of acceptor and donor electron of amino acids in bacteria indicated red color shows the negative place and blue color shows the positive place. Green box shows active site of bacteria which Ag has interaction with. Accessible pose for getting dock and binding site recognized by green box. In fact, for evaluating and predicting the accuracy of binding ability between ligands and target protein, the binding free energies (ΔG) for the docking models and the crystal struc-

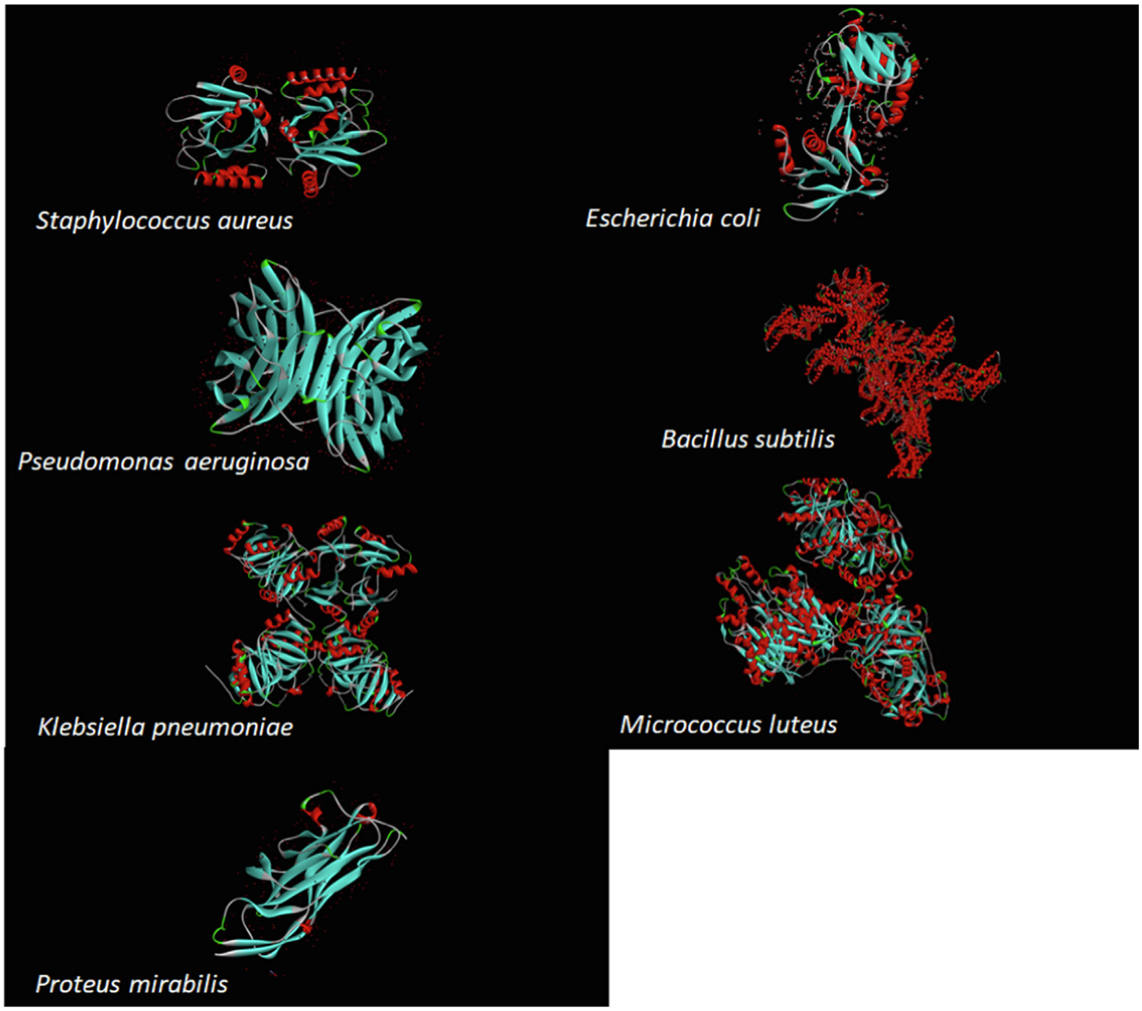

Fig. 11 Structure of all of applied bacteria.

tures were calculated. The lower binding energy value specify the binding strength of the ligands and docking model. Therefore, to calculate the binding strength of Ag, the Ag-bacteria docked complexes were analyzed based on minimum binding energy values and Ag interaction (hydrogen/hydrophobic) pattern. Docking results reported in Table 1 recognized that AgNPs had good interaction by bacteria and indicated antibacterial manner in solvent. According to the results lower binding energy is belonged to *Klebsiella pneumoniae* and *Escherichia coli*. Therefore strong interaction related to Ag with *Klebsiella pneumoniae* and *Escherichia coli*. Fig. 11 illustrates the structure of all of applied bacteria as well.

4. Conclusion

The present study reported green synthesis of silver nanoparticles (AgNPs) in the presence of various herbal extracted oils freely via a simple, green, economical and reliable biological oil-in-water nanoemulsion technique which recommend the industrial metal NPs production without applying any dangerous and unfriendly reducing, dispersing and capping agent. The TEM and XRD analysis of synthesized AgNPs revealed that size of nanoparticles is about ~52 nm by spherical shape formed in the presence of *Artemisia herba-alba*. MTT studies indicated anti-cancer activity against MCF-7 human breast cancer cells. Furthermore, according to the associated antimicrobial properties and stable nature of these nanoparticles, it was appeared that these nanoparticles are developed in numerous biomedical applications such as cosmetics well. Energy binding and activation pose of bacteria supported the experimental data with great accordance via docking theoretical investigation.

CRediT authorship contribution statement

Razieh Razavi: Methodology, Investigation, Software, Formal analysis. **Mahnaz Amiri:** Writing - original draft, Visualization, Formal analysis. **Hassan Abbas Alshamsi:** Software, Formal analysis. **Tuba Eslaminejad:** Software, Formal analysis. **Masoud Salavati-Niasari:** Validation, Investigation, Data curation, Conceptualization, Methodology, Supervision, Project administration, Resources.

Declaration of Competing Interest

The authors declare that they have no known competing financial interests or personal relationships that could have appeared to influence the work reported in this paper.

Acknowledgment

The authors were appreciative to Iran National Science Foundation council (INSF, 97017837) and University of Kashan for Grant No (159271/24) supporting.

References

Accelrys Software Inc., 2007. D. Studio, Version 4.1, Accelrys Software Inc, San Diego, CA.

Accelrys Software Inc., 2007. D. Studio, Version 4.1, Accelrys Software Inc, San Diego, CA.

Ahmed, Sh., Ahmad, M., Swami, B.L., Kram, S., 2016. A review on plants extract mediated synthesis of silver nanoparticles for antimicrobial applications: a green expertise. J. Adv. Res. 7, 17–28.

Amiri, M., Salavati-Niasari, M., Akbari, Ahmad, Razavi, R., 2016. Sol–gel auto-combustion synthesize and characterization of a novel anticorrosive cobalt ferrite nanoparticles dispersed in silica matrix. J. Mater. Sci: Mater. Electron. https://doi.org/10.1007/s10854-017-6823-8.

Amiri, M., Salavati-Niasari, M., Pardakhty, A., Ahmadi, M., Akbari, A., 2017. Caffeine: a novel green precursor for synthesis of magnetic CoFe2O4 nanoparticles and pH-sensitive magnetic alginate beads for drug delivery. Mater. Sci. Eng. C.76, 1085–1093.

Amiri, M., Salavati-Niasari, M., Akbari, A., Gholami, T., 2017. Removal of malachite green (a toxic dye) from water by cobalt ferrite silica magnetic nanocomposite: herbal and green sol-gel autocombustion synthesis. Int. J. Hydrogen Energy 42 (39), 24846–24860.

Amiri, M., Akbari, A., Ahmadi, M., Pardakhti, A., Salavati-Niasari, M., 2018. Synthesis and in vitro evaluation of a novel magnetic drug delivery system; proecological method for the preparation of CoFe2O4 nanostructures. J. Mole. Liquids 249, 1151–1160.

Amiria, M., Pardakhtib, A., Ahmadi-Zeidabadic, M., Akbaria, A., Salavati-Niasaria, M., 2018. Magnetic nickel ferrite nanoparticles: green synthesis by Urtica and therapeutic effect of frequency magnetic field on creating cytotoxic response in neural cell lines. Colloids Surfaces B: Biointerf. 172, 244–253.

Arokiyaraj, S., Arasu, M.V., Vincent, S., Prakash, N.U., Choi, S.H., Oh, Y.K., Choi, K.C., Kim, K.H., 2014. Rapid green synthesis of silver nanoparticles from Chrysanthemum indicum L and its antibacterial and cytotoxic effects: an in vitro study. Int. J. Nanomed. 9, 379–388.

Babu, S.A., Prabu, H.G., 2011. Synthesis of AgNPs using the extract of Calotropisprocera flower at room temperature. Mater. Lett. 65 (11), 1675–1677.

Bahadur, N.M., Furusawa, T., Sato, M., Kurayama, F., Siddiquey, I. A., Suzuki, N., 2011. Fast and facile synthesis of silica coated silver nanoparticles by microwave irradiation. J. Colloid Interface. Sci. 355 (2), 312–320.

Bastús, N.G., Merkoçi, F., Piella, J., Puntes, V., 2014. synthesis of highly monodisperse citrate-stabilized silver nanoparticles of up to 200 nm: kinetic control and catalic properties. Chem. Mater. 26, 2836–2846.

Beg, M., Maji, A., Mandal, A.K., Das, S., Aktara, M.N., Jha, P.K., Hossain, M., 2016. Green synthesis of silver nanoparticles using Pongamia pinnata seed: characterization, antibacterial property, and spectroscopic investigation of interaction with human serum albumin. J. Mol. Recognit. 8, 259–266.

Boopathi, S., Gopinath, S., Boopathi, T., Balamurugan, V., Rajeshkumar, R., Sundararaman, M., 2012. Characterization and antimicrobial properties of silver and silver oxide nanoparticles synthesized by cell-free extract of a mangrove-associated Pseudomonas aeruginosa M6 using two different thermal treatments. Ind. Eng. Chem. Res. 51 (17), 5976–5985.

Coseri, S., Spatareanu, A., Sacarescu, L., Rimbu, C., Suteu, D., Spirk, S., Harabagiu, V., 2015. Green synthesis of the silver nanoparticles mediated by pullulan and 6- carboxypullulan. Carbohydr. Polym. 116, 9–17.

Daengsakul, S., Mongkolkachit, C., Thomas, C., Siri, S., Thomas, I., Amornkitbamrung, V., Maensiri, S., 2009. A simple thermal decomposition synthesis, magnetic properties and cytotoxicity of $La_{0.7}$ $Zr_{0.3}$ MnO_3 nanoparticles. Appl. Phys. A 96, 691–699.

Dubey, S.P., Lahtinen, M., Sillanpaa, M., 2010. Green synthesis of gold and silver nanoparticles using Averrhoa bilimbi fruit extract. Process Biochem. 45, 1065–1071.

Elshikh, M., Ahmed, S., Funston, S., Dunlop, P., McGaw, M., Marchant, R., Banat, I.M., 2016. Resazurin-based 96-well plate microdilution method for the determination of minimum inhibitory concentration of biosurfactants. Biotechnol. Lett. 38 (6), 1015–1019.

Emadzade, K., Gehrke, B., Peter Linder, H., Hörandl, E., 2011. The biogeographical history of the cosmopolitan genus *Ranunculus* L (Ranunculaceae) in the temperate to meridional zones. Mol. Phylogenet. Evol. 58 (1), 4–21.

Eslaminejad, T., Nematollahi-Mahani, S.N., Ansari, M., 2016. Synthesis, characterization, and cytotoxicity of the plasmid EGFP-p53 loaded on pullulan–spermine magnetic nanoparticles. J. Magnetism Magnetic Mater. 402, 34–43.

Eslaminejad, T., Nematollahi-Mahani, S.N., Ansari, M., 2016. Cationic β-cyclodextrin–chitosan conjugates as potential carrier for pmCherry-C1 gene delivery. Mole. Biotechnol. 58 (4), 287–298.

Gogoi, N., Babu, P.J., Mahanta, C., Bora, U., 2015. Green synthesis and characterization of silver nanoparticles using alcoholic flower extract of Nyctanthes arbortristis and in vitro investigation of their antibacterial and cytotoxic activities. Mater. Sci. Eng. C 46, 463–469.

Hudaib, M.M., Aburjai, T.A., 2006. Composition of the essential oil from Artemisia herbaalba grown in Jordan. J. Essent. Oil Res. 18 (3), 301–304.

Ishiwatari, S., Suzuki, T., Hitomi, T., Yoshino, T., Matsukuma, S., Tsuji, T., 2007. Effects of methyl paraben on skin keratinocytes. J. Appl. Toxicol. 27, 1–9.

Jiang, K., Pinchuk, A.O., 2015. Noble metal nanomaterials: synthetic routes, fundamental properties, or1 promising applications. Solid State Phys. Adv. Res. Appl. 5, 131–211.

Justin Packia Jacob, S., Finub, J.S., Narayanan, Anand, 2012. Synthesis of silver nanoparticles using Piper longum leaf extracts and its cytotoxic activity against Hep-2 cell line. Colloid. Surface B. 91, 212–214.

Kacurakova, M., Capek, P., Sasinkova, V., Wellnes, N., Ebringerova, A., 2000. FT-IR study of plant cell wall model compounds: pectic polysaccharides and hemicelluloses. Carbohydr. Polym. 43, 195–203.

Kshirsagar, P., Sangaru, S.S., Malvindi, M.A., Martiradonna, L., Cingolani, R., Pompa, P.P., 2011. Synthesis of highly stable silver nanoparticles byphotoreduction and their size fractionation by phase transfer method. Colloids. Surf. A 392 (1), 264–270.

Kumar, B., Smita, K., Cumbal, L., Debut, A., 2017. Green synthesis of silver nanoparticles using Andean blackberry fruit extract. Saudi J. Biol. Sci. 24 (1), 45–50.

Kyte, Jack, Doolittle, Russell F., 1982. A simple method for displaying the hydropathic character of a protein. J. Mole. Biol. 157 (1), 105–132.

Lee, Kuen Yong, Mooney, David J., 2012. Alginate: properties and biomedical applications. Prog. Polym. Sci. 37 (1), 106–126.

Li, P., Li, S., Wang, Y., Zhang, Y., Hana, G., 2017. Green synthesis of CD-functionalized monodispersed silver nanoparticles with ehanced catalytic activity. Colloids Surf. A: Physicochem. Eng. Aspects 520, 26–31.

Majeed, S.h., Abdullah, M., Nanda, A., Ansari, M.T., 2016. In vitro study of the antibacterial and anticancer activities of silver nanoparticles synthesized from Penicilliumbrevicompactum. J. Taibah Univ. Sci. 10, 614–620.

Morris, G.M., Huey, R., Lindstrom, W., Sanner, M.F., Belew, R.K., Goodsell, D.S., Olson, A.J., 2009. AutoDock4 and AutoDockTools4: automated docking with selective receptor flexibility. J. Comput. Chem. 30, 2785–2791.

Naghdi, M., Taheran, M., Brar, S.K., Verma, M., Surampalli, R., Valero, J., 2015. 450 Green and energy-efficient methods for the production of metallic nanoparticles. Beilstein J. Nanotechnol. 6, 2354–2360.

Ocsoy, Ismail, Demirbas, Ayse, McLamore, Eric S., Altinsoy, Berrak, Ildiz, Nilay, Baldemir, Ayse, 2017. Baldemir, Green synthesis with incorporated hydrothermal approaches for silver nanoparticles formation and enhanced antimicrobial activity against bacterial and fungal pathogens. J. Mol. Liq. 238, 263–269.

Pal, Sukdeb, Tak, Yu Kyung, Song, Joon Myong, 2007. Does the antibacterial activity of silver nanoparticles depend on the shape of the nanoparticle? A study of the gram-negative bacterium escherichia coli. Appl. Environ. Microbiol. 73 (6), 1712–1720.

Rai, M., Yadav, A., Gade, A., 2009. Silver nanoparticles as a new generation of antimicrobials. Biotechnol. Adv. 27, 76–78.

Raja, S., Ramesh, V., Thivaharan, V., 2017. Green biosynthesis of silver nanoparticles using Calliandrahaematocephala leaf extract, their antibacterial activity and hydrogen peroxide sensing capability. Arab. J. Chem. 10, 253–261.

Rajkuberan, Chandrasekaran, Sudha, Kannaiah, Sathishkumar, Gnanasekar, Sivaramakrishnan, Sivaperumal, 2015. Antibacterial and cytotoxic potential of silver nanoparticles synthesized using latex of Calotropis gigantea L. Spectrochim. Acta. Part A 136, 924–930.

Rani, P.S., Rajasekharredy, P., 2011. Green synthesis of silver-protein (core–shell) nanoparticles using Piper betle L. leaf extract and its biological applications. Physicochem. Eng. Aspects 389, 188–194.

A. Rizwan, Protein Purification, 2012. InTech. ISBN 978-953-307-831-1.

Roszak, Joanna, Smok-Pieniążek, Anna, Domeradzka-Gajda, Katarzyna, Grobelny, Jarosław, Tomaszewska, Emilia, Ranoszek-Soliwoda, Katarzyna, Celichowski, Grzegorz, Stępnik, Maciej, 2017. Inhibitory effect of silver nanoparticles on proliferation of estrogendependent MCF-7/BUS human breast cancer cells induced by butyl paraben or di-n-butyl phthalate. Toxicol. Appl. Pharmacol. 337, 12–21.

Silver, S., Phung, L.T., Silver, G., 2006. Silver as biocides in burn and wound dressings and bacterial resistance to silver compounds. J. Ind. Microbiol. Biotechnol. 33, 627–634.

Singh, P., Kim, Y.J., Yang, D.C., 2015. A strategic approach for rapid synthesis of gold and silver nanoparticles by Panax ginseng leaves. Artifical Cells Nanomed. Biotechnol. https://doi.org/10.3109/21691401.2015.1115410.

Singh, R., Shushni, M.A.M., Belkheir, A., 2015. Antibacterial and antioxidant activities of Mentha piperita. L. Arab.J Chem. 8, 322–328.

Solmon, M.M., Umoren, S.A., 2016. In-situ preparation, characterization and anticorrosion property of polypropylene glycol/silver nanoparticles composite form lid steel corrosion in acid solution. J. Colloid Interface Sci. 462, 29–41.

Sura, U.K., Ankamwarb, B., Karmakarc, S., Halderc, A., Dasa, P., 2018. Green synthesis of Silver nanoparticles using the plant extract of Shikakai and Reetha. Mater. Today: Proc. 5, 2321–2329.

Surya, S., Dinesh Kumar, G., Rajakumar, R., 2016. Green synthesis of silver nanoparticles from flower extract of Hibiscus rosa-sinensis and its antibacterial activity. Int. J. Innov. Res. Sci. Eng. Technol. 5, 5242–5247.

Tadros, T., Izquierdo, P., Esquena, J., Solans, C., 2004. Formation andstability of nano-emulsions. Adv. Colloid Interface Sci. 108-109, 303–318.

Tilaoui, M., Ait-Mouse, H., Jaafari, A., Aboufatima, R., Chait, A., Zyad, A., 2011. Chemical composition and antiproliferative activity of essential oil from aerial parts of a medicinal herb Artemisia herba-alba. Braz. J. Pharm. 21, 781–785.

Valli, G., Suganya, M., 2015. Silver nanoparticles synthesis using Delonixelata flower extract by biogenic approach. Int. J. Pharmac. Chem. Biol. Sci. 5, 567–571.

Varadavenkatesan, T., Vinayagam, R., Selvaraj, R., 2017. Structural characterization of silver nanoparticles phyto-mediated by a plant waste, seed hull of vinga mungo and their biological applications. J. Mol. Struct. 5, 629–635.

Vernin, G., Merad, O., Vernin, G.M., Zamkotsian, R.M., Parkanyi, C. D., 1995. GC–MS analysis of Artemisia herba-alba. Essential oils from Algeria. Dev. Food Sci. 37, 147–205.